Speckle Interferometry of binary stars with a 1m telescope, grounded with AO from a 1.5m

Tanya Tavenner, Jack Drummond[†], Mala Mateen
Ethan Wood, Odell Reynolds Emory Jenkins[††]
Air Force Research Laboratory, RDSS, Starfire Optical Range
[†]*also Leidos,* [††]*AFRL Summer Internship*

ABSTRACT

Speckle interferometry observations of about a dozen binary stars of 5th to 9th magnitude in the I-band (0.9 microns) were made with a 1 m telescope at the Starfire Optical Range on two nights, 2020 Nov 3 and 2021 Feb 23. The binaries had separations ranging from the telescope diffraction limit to more than one arcsec, and included a variety of magnitude differences. Parametric Blind Deconvolution (PBD) is demonstrated to extract orientations, separations, and magnitude differences from the mean FFTs of the centered short exposure images. PBD can also be applied to the mean centered shift-and-add images. While the orientation and separations are relatively easy to measure and can be compared to catalog information, the magnitude differences are not only difficult to determine, they are not readily available from the literature for any particular wavelength. Therefore, we also obtained adaptive optics observations at the same wavelength with a nearby 1.5 m telescope on the second night to provide ground truth. The results from these observations are directly applicable to closely spaced objects (CSO), satellites at geosynchronous distances, all of which are point sources from the ground.

1. INTRODUCTION

Before adaptive optics there was speckle interferometry. For high angular resolution astronomy, adaptive optics (AO) is superior in many ways, but speckle interferometry (SI) [1] can perform just as well on simple point sources, such as binary stars or closely spaced objects (CSO), e.g., man-made satellites. The Starfire Optical Range (SOR), the cradle if not the birthplace of AO [2] [3], has several AO systems on telescopes, but also has other non-AO smaller (1 m) telescopes, as do many Air Forces sites scattered around the world. Therefore, we undertook a series of observations utilizing SI on a 1 m telescope, and compared the technique to AO observations on our 1.5 m telescope to see if SI, which is much less expensive, is suitable for CSO work on 1 m class telescopes.

2. SPECKLE INTERFEROMETRY

The method of Speckle Interferometry (SI) is to obtain short exposure (0.01 second) images that freeze the atmosphere before they become blurred and then stack the individual complex FFTs, or their power spectra [1]. In our case, we first center each image on its brightest pixel, form its FFT, and then save the sum of the FFTs to create an average FFT over 1000-40000 frames, F_0. Each short exposure image contains multiple speckles all of which show the binary to some extent. Each FFT (and the mean of the FFT's) will then reveal fringes from the binary on top of the speckle transfer function. Inverting F_0 brings the Fourier plane signal back to the image domain, $I_0 = \mathrm{FFT}^{-1}(F_0)$.

Equivalently, designating individual centered images as i_0, we can form the mean of n centered images, I_0, and then take the FFT,

$$\mathrm{FFT}(I_0) = \mathrm{FFT}(\Sigma i_0/n) = \Sigma(\mathrm{FFT}(i_0))/n = F_0 \quad , \tag{1}$$

or inverting,

$$I_0 = \Sigma i_0/n = \mathrm{FFT}^{-1}(\Sigma(\mathrm{FFT}(i_0))/n) = \mathrm{FFT}^{-1}(F_0) \quad . \tag{2}$$

Approved for public release; distribution is unlimited. Public Affairs release approval AFRL-2021-2761

The mean image I_0, or the mean FFT F_0, can be fit for two point spread functions (PSF). Fitting I_0 as Lorentzians, Gaussians, and Airy functions reveals, in Fig. 1, that a Lorentzian (L) seems to be the best description of the PSF produced by the atmosphere and telescope [4] [5]. Therefore, we fit a binary as two Lorentzians in either the image plane or in the frequency plane, where the Fourier transform of a Lorentzian is a modified Bessel function of the second kind of order 0, $K0$. Thus, we can fit I_0 in the image plane as two Lorentzians, L_1+L_2, or F_0 in the frequency plane as $K0_1$+$K0_2$. Here we fit in the frequency domain, fitting the real and imaginary parts of F_0 rather than the modulus and phase. This method of fitting binary stars as two Lorentzians (or any functional form) in order to extract parameters does not require separately measuring a PSF, and therefore, is called Parametric Blind Deconvolution or PBD [4] [5]. PBD can be used where the object is simple and symmetric, such as these binaries, or asteroids [6] [7] modeled as flat triaxial ellipses. Mathematical expressions are given in [4] [5] [6] and [7].

One trick that is essential to the fit of the accumulated centered image I_0 is to subtract the background obtained in the fit of F_0 from the center pixel in I_0 before it is in turn fit as a pair of Lorentzians. This background is the noise floor in the FFT, and is the single pixel noise in the image center pixel.

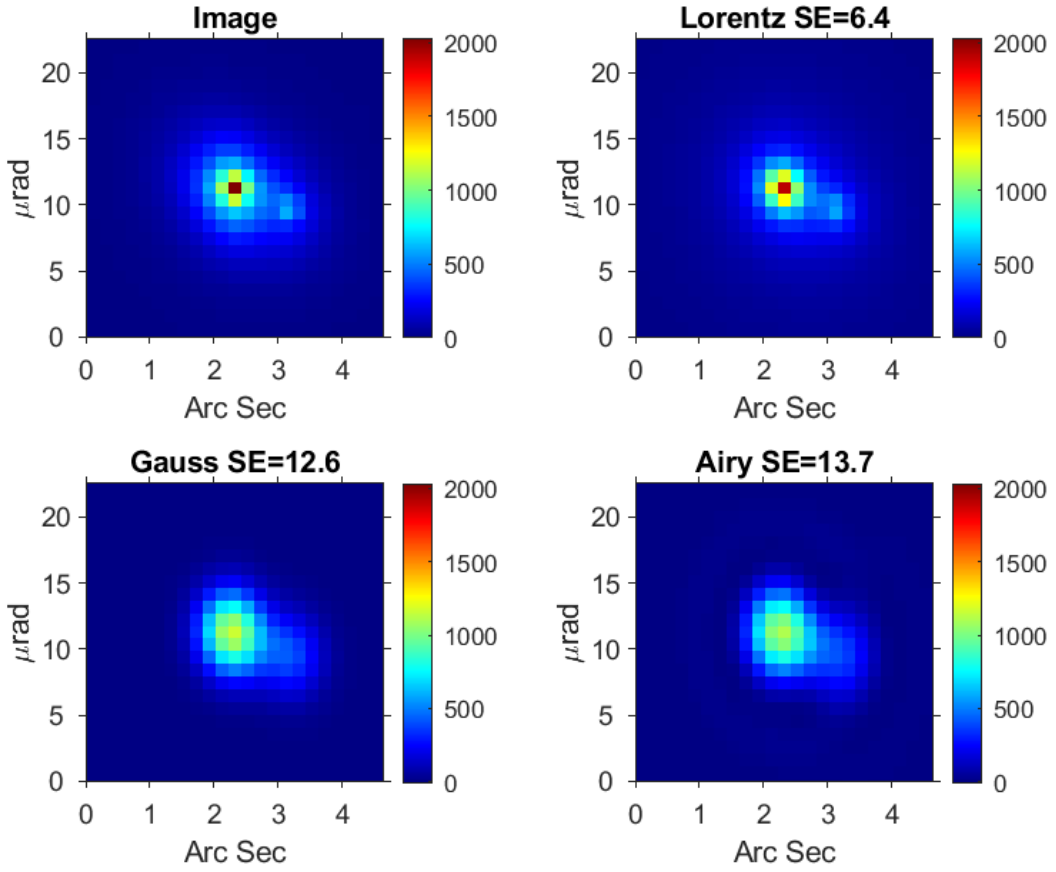

Fig. 1: Image (I_0) of HIP 102589 and three functional fits. The SE in the title is the Standard Error of Fit in counts, and can be compared to the pixel counts in the colorbar. Clearly the Lorentz function fits the binary better than the Gauss and Airy fits.

While the goal was to measure binary stars down to the diffraction limit of our D=1 m diameter telescope, $\theta = \lambda/D = 0.165''$, our image pixel scale was too large, $0.2''$/pix, to make a serious challenge to the telescope's resolution. The Nyquist theorem states that it takes two pixels across the diffraction limit, a rexel, to resolve two objects, which means that our effective resolution is twice the pixel scale, $0.4''$. See Fig. 2 for an illustration of the situation, where the rexel falls completely inside a pixel. However, with the prior knowledge that the objects are two stars with Lorentzian shape, we can perhaps resolve point sources to below the pixel scale, but probably not to the diffraction limit.

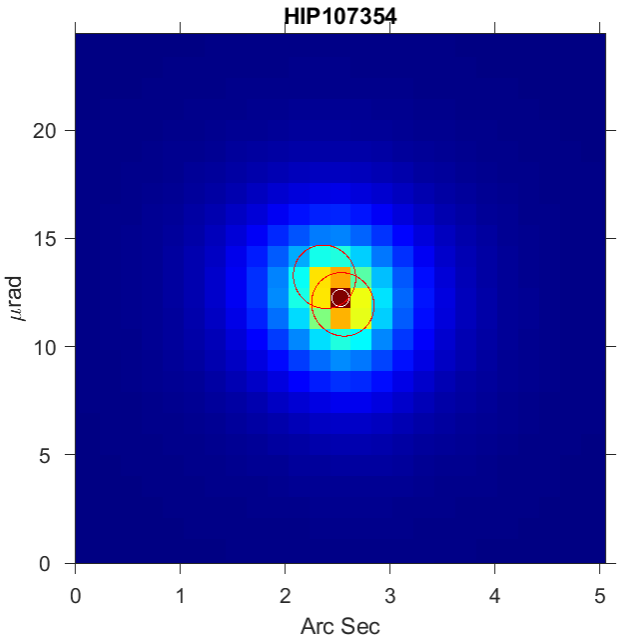

Fig. 2: Closest binary from 2020 Nov 3. Two red ellipses delineate the FWHM of the Lorentzian PSF for the two stars from the image plane fit of HIP 107354, and the size of the diffraction limit of the 1 m telescope, a rexel, is shown as a circle on the middle pixel.

3. TWO NIGHTS

We began our foray into SI with relatively bright and wide binaries having small brightness differences (Δmags) on 2020 Nov 4, using the Sixth Catalog of Orbits of Visual Binary Stars (6th Orbit Catalog, hereafter, or simply, the catalog), available at the US Naval Observatory[1] for comparison. Since HIP 118281 does not have an orbit in the catalog, we used parameters from the latest observation in the Washington Double Star Catalog (WDS), also available from the US Naval Observatory.

For the second round, on 2021 Feb 23, we chose fainter and closer binaries with greater Δmags. On this second night, we also had our 1.5 m telescope image the same objects with adaptive optics for comparison. While the 6th Orbit Catalog provided reliable separations and orientations from orbits, Δmags are uncertain partly because the wavelength for the Δmags are not reported. However, the 1.5 m AO images obtained at λ_0=0.9μm give us 'exact' parameters measured the same week at our 1 m telescope with λ_0=0.8μm.

Fig. 3 shows F_0, I_0, and the model fits to both for the ten binaries observed on 2020 Nov 4 and listed in Table 1. Actually, since it is not possible to sensibly display a complex image, we show the log(abs(F_0)) and its model, even though the fit is performed on the real and imaginary parts of the F_0. The inverse FFT of F_0 is shown in the 3rd row of Fig. 3 to compare to I_0 and its model in the following rows, all shown for each binary on a linear intensity scale, and illustrating Eq 2. For the 7th and 10th binaries, centering on the brightest pixel sometimes resulted in the secondary appearing brighter than the primary for small Δmag cases, swapping the positions of the pair. Therefore, we made another pass on them with a modified shift-and-add centering algorithm to force the correct orientation before adding; these results are in Table 1, but are not illustrated in Fig. 3.

Fig. 4 shows the eight binaries for 2021 Feb 23 and listed in Table 2, with an additional row showing the AO images from the 1.5 m. There is a difference in some binary parameters between the catalog and the 1.5 m AO images, sometimes an indication that the orbit needs to be updated. Therefore, for 2021 Feb 23, we compare the SI results to AO, rather than the catalog, in the last row of Fig. 4. The line through Table 2 demarcating 0.4″shows the Nyquist sampling limit, below which the Δmags become particularly unreliable when compared to the 1.5 m AO images.

[1] https://www.usno.navy.mil/USNO/astrometry/optical-IR-prod/wds

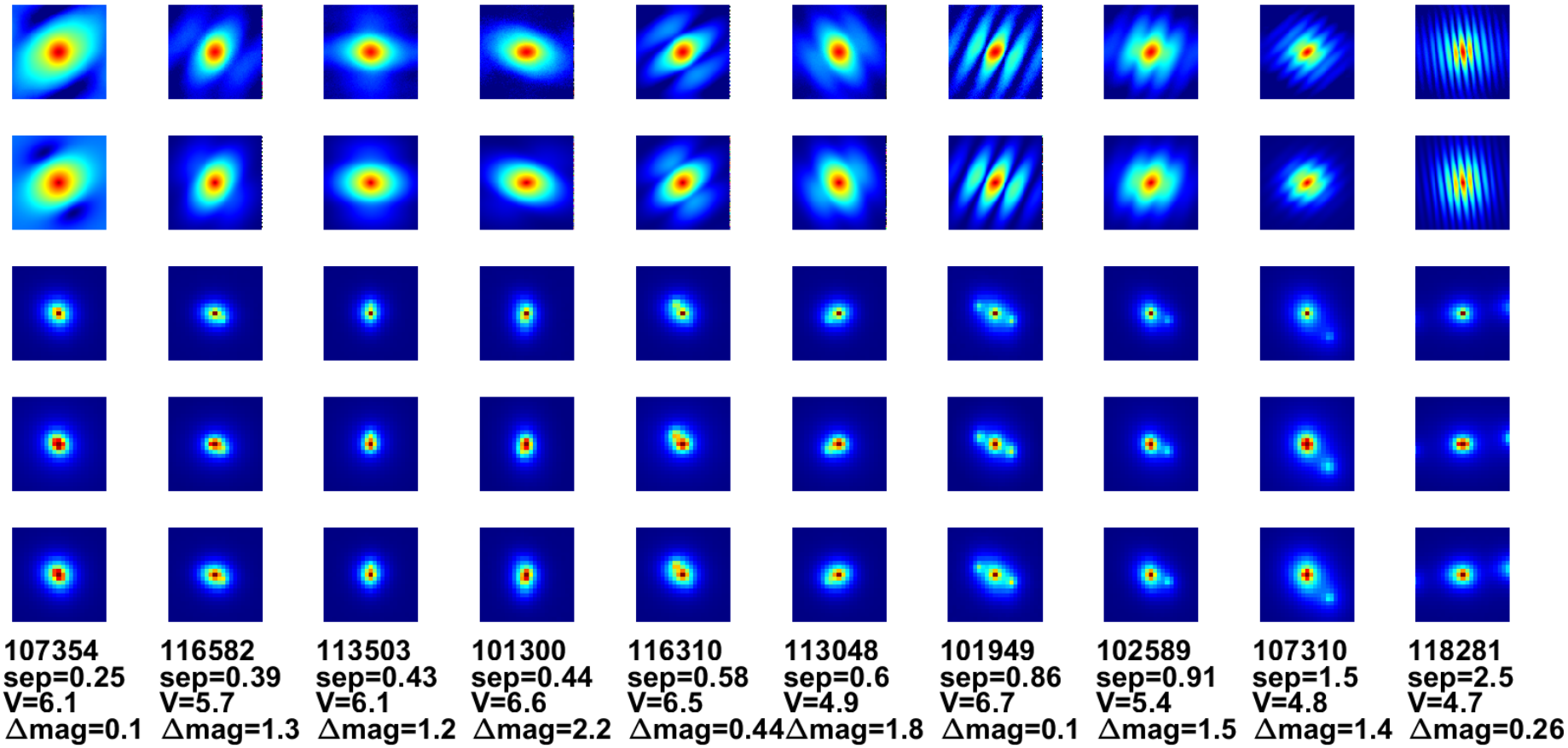

Fig. 3: 2020 Nov 4. Mean FFT (F_0) of centered shift-and-add images, i_0, and mean images I_0 of 10 binaries, ordered left to right, from smallest to largest catalog separations. Top row: The log(abs(F_0)). Fringes appear on top of the speckle transfer function; the closer the separations the fewer and further apart are the fringes. Second row: Least squares fit model of the top row. Third row: Mean images I_0. Fourth row: Least squares fit model of I_0 images. Fifth Row: Inverse FFT of F_0. Sixth row: Hipparcos number, catalog values of separations in arcsec, V_1 magnitude of the primary, and magnitude differences between the two. The field of view is $4.5''$for the images in the 3rd, 4th, and 5th rows. For the 7th and 10th binaries, centering on the brightest pixel sometimes resulted in the secondary appearing brighter than the primary for small Δmag cases, swapping the positions of the pair.

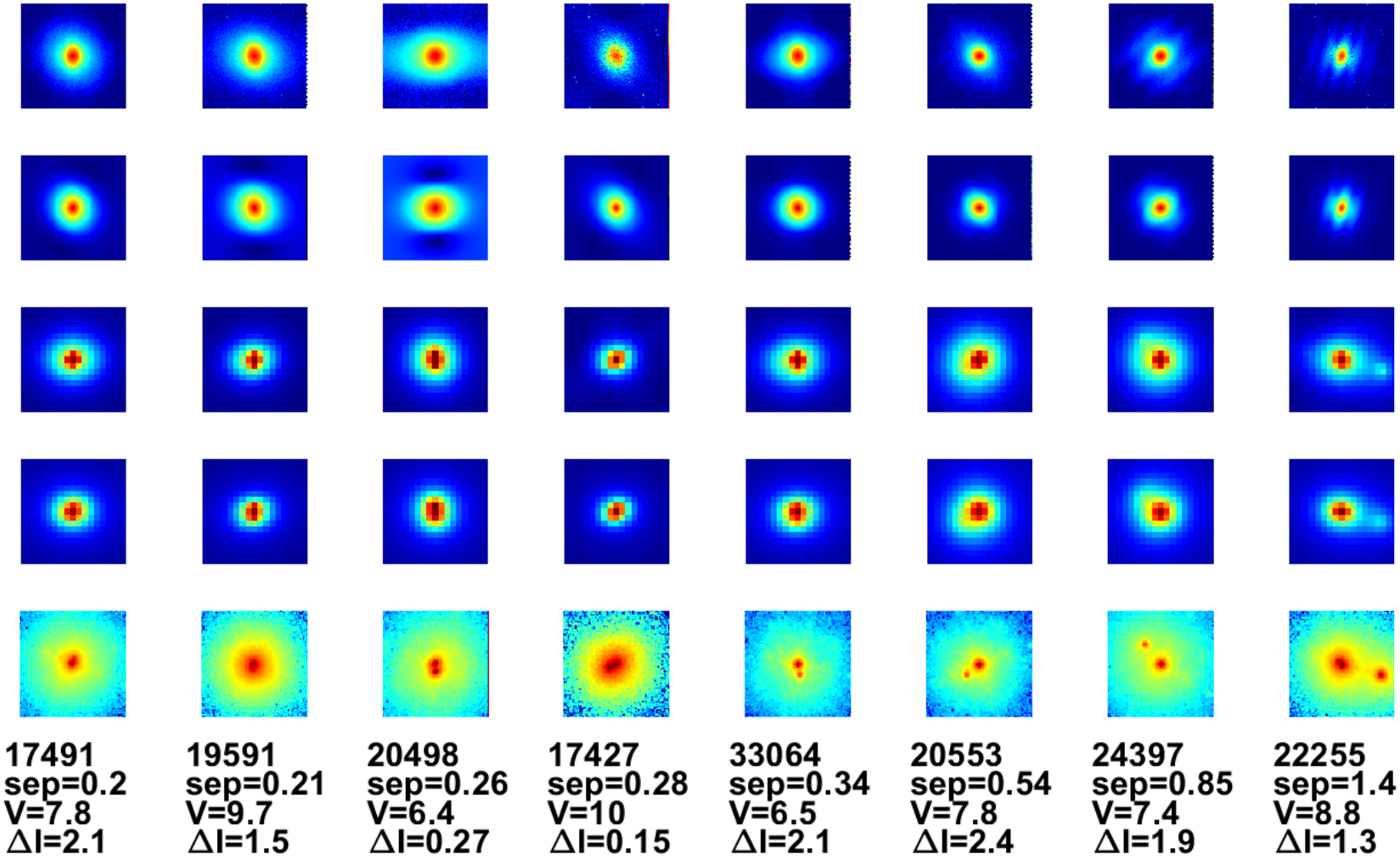

Fig. 4: 2021 Feb 23. Same as Fig. 3, but the fifth row now contains 1.5 m telescope adaptive optics images (instead of the FFT^{-1}), on a log scale, oriented to the same direction as the SI figures. The AO images are the same width as the SI I_0 images, 3.5″, slightly smaller than in Fig. 3. In the last row the separations and ΔI are from these AO images rather than from the catalog.

Table 1: 2020 Nov 4 Binary Star Information. For each binary star observed, its Hipparcos number is listed, followed by the V magnitude of the primary, V_1, and the magnitude difference between the pair, Δmag, from the 6th Orbit Catalog , followed by the position angle (PA) of the secondary and the separation in arcsec between the two stars calculated from the orbit listed in the catalog. The Δmag, PA, and separation as measured with speckle interferometry (SI) on our 1 m telescope are in the last three columns. The table is ordered by separation and matches Fig. 3.

Hipparcos number	Cat V_1	Cat Δmag	Cat PA (°)	Cat sep (″)	1 m SI Δmag	1 m SI PA (°)	1 m SI sep (″)
107354	4.94	0.10	301.3	0.251	0.07 ± 0.02	294.5 ± 0.5	0.361 ± 0.003
116582	6.08	1.30	22.5	0.389	0.88 ± 0.02	17.2 ± 0.5	0.450 ± 0.003
113503	6.11	1.16	37.9	0.430	1.00 ± 0.01	33.6 ± 0.4	0.418 ± 0.003
101300	6.58	2.17	258.5	0.438	0.58 ± 0.03	254.8 ± 0.6	0.369 ± 0.003
116310	5.67	0.44	107.6	0.581	0.55 ± 0.01	108.7 ± 0.2	0.574 ± 0.002
113048	5.97	1.82	251.0	0.597	1.07 ± 0.01	249.8 ± 0.3	0.552 ± 0.002
101949	6.73	0.10	3.2	0.862	0.13 ± 0.01	3.4 ± 0.1	0.864 ± 0.002
102589	4.73	1.53	0.1	0.908	1.48 ± 0.01	1.0 ± 0.2	0.877 ± 0.003
107310	4.75	1.43	323.3	1.513	1.35 ± 0.01	323.1 ± 0.1	1.500 ± 0.003
118281*	6.46	0.26	342.6	2.487	0.17 ± 0.00	341.9 ± 0.0	2.521 ± 0.002

*The information for HIP 118281 is from the WDS, since it does not have an orbit in the 6th Orbit Catalog.

Table 2: 2021 Feb 23 Binary Star Information. The same as Table 1, but with the Δmag, PA, and separation as measured on AO images obtained at the 1.5 m added, with uncertainties of ≤ 0.02 mags, 0.6°, and 0.002″, respectively. The table matches the order in Fig. 4. The line through the table demarcates 0.4″, above which our SI measurements are unreliable, particularly in the Δmags.

Hipp number	Cat V_1	Cat Δmag	Cat PA (°)	Cat sep (″)	AO Δmag	1.5 m PA (°)	AO sep (″)	1 m SI Δmag	1 m SI PA (°)	1 m SI sep (″)
17491	7.80	2.70	113.3	0.143	2.08	107.9	0.196	0.25 ± 0.07	108.6 ± 1.7	0.295 ± 0.006
19591	9.68	2.11	228.7	0.172	1.51	224.4	0.207	-0.05 ± 0.03	236.8 ± 0.9	0.319 ± 0.003
20498	6.38	2.03	134.2	0.254	0.27	134.9	0.264	-0.21 ± 0.03	130.1 ± 0.7	0.411 ± 0.004
17427	10.07	0.31	88.2	0.272	0.15	88.6	0.282	0.01 ± 0.07	112.0 ± 1.9	0.308 ± 0.008
33064	6.47	2.49	303.0	0.383	2.08	305.4	0.343	0.63 ± 0.04	297.4 ± 1.0	0.387 ± 0.004
20553	7.78	3.02	228.5	0.549	2.39	230.5	0.543	1.44 ± 0.03	230.2 ± 0.7	0.699 ± 0.008
24397	7.43	2.51	177.0	0.805	1.91	176.4	0.854	1.46 ± 0.02	182.5 ± 0.6	0.780 ± 0.007
22255	8.78	1.28	22.0	1.400	1.25	18.4	1.404	1.40 ± 0.02	19.1 ± 0.3	1.341 ± 0.008

A closer look at the 1.5 m AO images (Fig. 5), the ground truth for Feb 2021, shows that the first two binaries are hard to see in the images, but the fringe signature of the binaries are visible in their FFTs. Also prominent in Fig. 5 is the high frequency cutoff that separates signal from noise. For a pixel scale with Nyquist sampling this cutoff would just touch the edge of the frame, but since the cutoff is well inside, the 1.5 m is slightly over-sampled. The FFTs from the 1 m telescope in Figs. 3 and 4 show no sign of the cutoff, indicating that the diffraction limit is under-sampled for the 1 m telescope; it would be a 244 pixel diameter circle on the 101x101 pixel FFTS in Figs. 3 and 4.

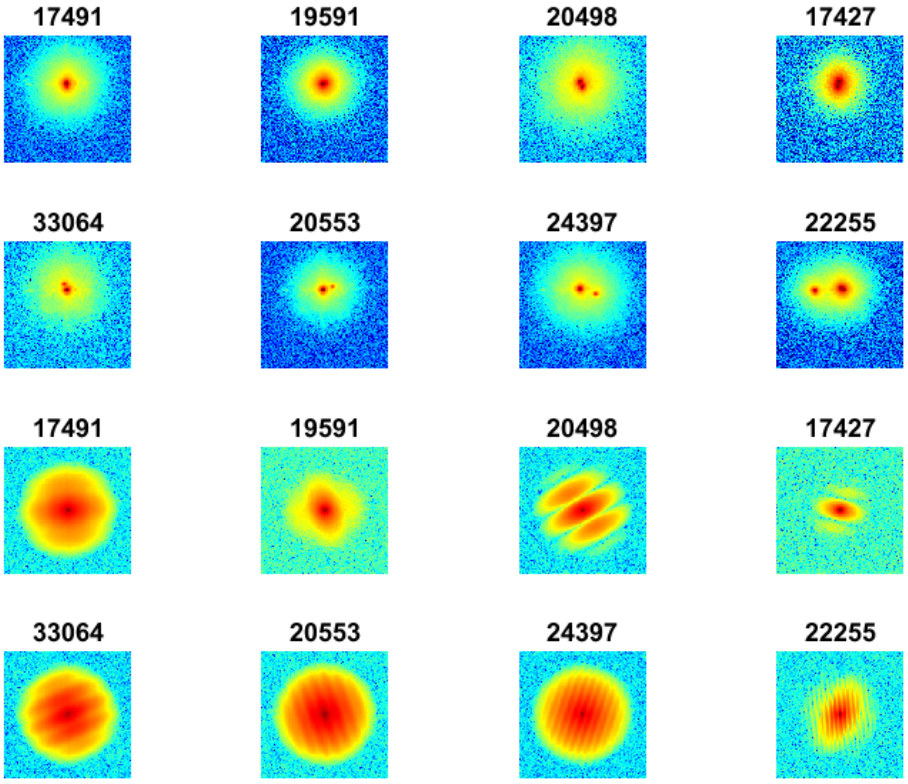

Fig. 5: Adaptive optics images from the 1.5 m telescope on 2021 Feb 23. Top two rows: AO images from the 1.5 m with Hipparcos numbers, shown on a log intensity scale. The width of the images is 6.5″. Bottom two rows: the FFT of the images shown in the first two rows, shown as the log of the modulus, log(abs(FFT(image))). Except for the first two binaries with separations of 0.2″, near the 0.12″diffraction limit of the 1.5 m telescope, all of the AO images and their FFTs easily show the the two stars. The high frequency cutoff clearly visible as the demarcation between the signal and noise in the FFTs indicates that the 1.5 m telescope slightly over-samples the diffraction limit.

4. DISCUSSION

For the bright wide binaries observed in November 2020, the comparison between SI and the catalog is very good, with the only real discrepancy being between the Δmags, where the ones from the catalog are from unspecified sources and wavelengths. The separations measured with 9 of the 10 binaries yield a pixel scale of 0.198±0.002″/pixel, the same as previously obtained with images of wide binaries. Fig. 6 shows the separations from both nights. While all but one of the Nov 2020 binaries had measured separations greater than twice the pixel scale, only 3 of the 8 binaries

from Feb 2021 had separations greater than the 0.4″pixels. Nevertheless, all of the separations from both nights fall along the image scale line.

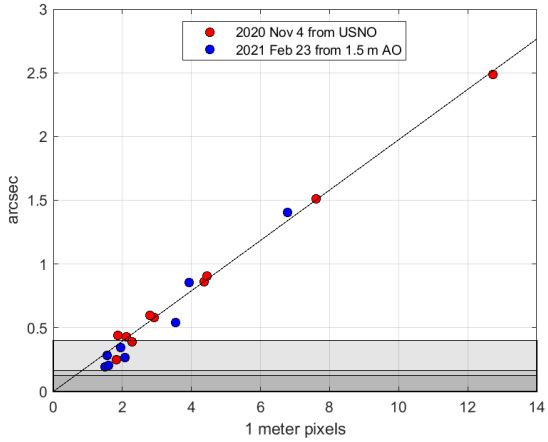

Fig. 6: Binary star separations. A comparison of measured separations from SI in pixels to catalog (Nov 2020) or 1.5 m measured separations (Feb 2021) . The straight line is a fit to 9 of the 10 binaries from Nov 2020, and yields the pixel scale of 0.198±0.002″/pixel. The Nyquist limit for resolution of two pixels is shown as the gray area below 0,4″, and below that is the 1 m telescope diffraction limit at 0.0165″, and below that is the 1.5 m diffraction limit of 0.124″.

In Fig 7 a trend in the Δmags is observed in that the greater the catalog or AO Δmags the larger is the difference between them and the SI Δmags, *i.e.*, the SI Δmags increasingly underestimate the true Δmags, especially above a true Δmag of 1.5. The same thing occurs as separations approach 0.4″. The situation is less clear when considering the brightness of the primary. Stating this another (obvious) way, the further apart and the smaller the Δmags, the easier is the problem and the better is the agreement between catalog, AO, and SI Δmags.

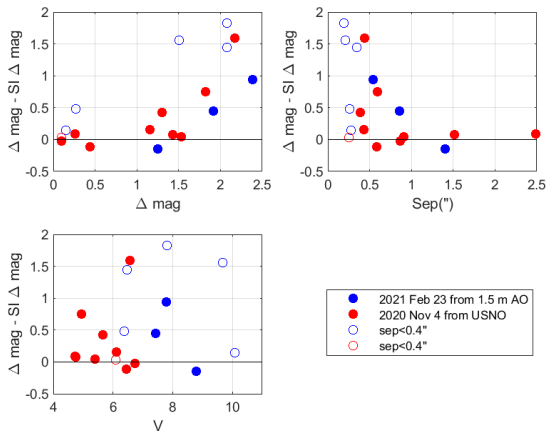

Fig. 7: Δmagnitude comparisons. The difference between true (catalog or AO) Δmags and SI Δmags (upper left) appears to be a strong function of true Δmags above a true Δmag of 1.5, and as the separations approach the Nyquist sampling limit of 0,4″(upper right). The difference between the Δmags does not appear to be a function of the primary star's magnitude (lower left), with a formal correlation coefficient of 0.26.

5. SUMMARY

Part of the power of speckle interferometry lies in the centering of the short exposure images with shift-and-add (SAA) [8] [9], a cousin of 'lucky imaging' (where only the best and brightest short exposures are used). Evidently, even this simple stacking of images approaches a telescope and camera resolution limit, but we were clearly handicapped by large camera pixels. Pixels that under-sample the diffraction limit by a factor of 2.4, *i.e.*, images where two pixels span 2.4 resolution elements, or rexels, are not conducive to high angular resolution astronomy.

In the end, only the widest three binaries from Feb 2021 can be considered good measurements, compared to 9 of 10 from Nov 2021. Also, no results could be obtained from observations of two other binaries fainter than $V_1 > 10$, perhaps indicating a need for exposures longer than 0.01 s. However, we have demonstrated resolution below the normal atmospheric seeing of 1-2″, leaving SI as a reasonable method to improve resolution, but with unreliable brightness differences, for day-to-day operations.

Acknowledgments

We appreciate discussions with Julian Christou on speckle interferometry, especially on shift-and-add methods, even though he made fun of us. Julian coined the term Parameteric Blind Deconvolution some 25 years ago.

We thank the expert staff at the SOR for assisting us with our observations, especially James Mathis and Scott Newey.

REFERENCES

[1] Labeyrie, A. 1970. Attainment of Diffraction Limited Resolution in Large Telescopes by Fourier Analysing Speckle Patterns in Star Images. *Astronomy and Astrophysics* 6, 85.

[2] Fugate, R. Q., Wopat, L. M., Fried, D. L., Ameer, G. A., Browne, S. L., Roberts, P. H., Tyler, G. A., Boeke, B. R., Ruane, R. E. 1991. Measurement of atmospheric wavefront distortion using scattered light from a laser guide-star. *Nature* 353, 144–146.

[3] Duffner, R. W 2009. *The Adaptive Optics Revolution: A History.* Albuquerque: University of New Mexico Press, 2009.

[4] Drummond, J. D. 1998. Adaptive optics Lorentzian point spread function. Adaptive Optical System Technologies, *SPIE* 3353, 1030-1037.

[5] Drummond, J. D. 2014. Binary Stars Observed with Adaptive Optics at the Starfire Optical Range. *The Astronomical Journal* 147, 65.

[6] Drummond, J. D., Fugate, R. Q., Christou, J. C., Hege, E. K., 1998. Full Adaptive Optics Images of Asteroids Ceres and Vesta; Rotational Poles and Triaxial Ellipsoid Dimensions. *Icarus* 132, 80–99.

[7] Drummond, J. D. and 11 colleagues 2018. The triaxial ellipsoid size, density, and rotational pole of asteroid (16) Psyche from Keck and Gemini AO observations 2004-2015. *Icarus* 305, 174-185.

[8] Christou, J. C., Ribak, E., Hege, E. K., Freeman, J. D. 1986. Images from astronomical speckle data: weighted shift-and-add analysis.. *Optical Engineering* 25, 724-730.

[9] Christou, J. C., Hege, E. K., Freeman, J. D., Ribak, E. 1986. Self-calibrating shift-and-add technique for speckle imaging. *Journal of the Optical Society of America A* 3, 204-209.